
Neural Image Compression and Explanation

Xiang Li

Department of Computer Science
Georgia State University
Atlanta, GA 30302
xli62@student.gsu.edu

Shihao Ji

Department of Computer Science
Georgia State University
Atlanta, GA 30302
sji@gsu.edu

Abstract

Explaining the prediction of deep neural networks (DNNs) and semantic image compression are two active research areas of deep learning with a numerous of applications in decision-critical systems, such as surveillance cameras, drones and self-driving cars, where interpretable decision is critical and storage/network bandwidth is limited. In this paper, we propose a novel end-to-end Neural Image Compression and Explanation (NICE) framework that learns to (1) explain the prediction of convolutional neural networks (CNNs), and (2) subsequently compress the input images for efficient storage or transmission. Specifically, NICE generates a sparse mask over an input image by attaching a stochastic binary gate to each pixel of the image, whose parameters are learned through the interaction with the CNN classifier to be explained. The generated mask is able to capture the saliency of each pixel measured by its influence to the final prediction of CNN; it can also be used to produce a mixed-resolution image, where important pixels maintain their original high resolution and insignificant background pixels are subsampled to a low resolution. The produced images achieve a high compression rate (e.g., about 0.6x of original image file size), while retaining a similar classification accuracy. Extensive experiments across multiple image classification benchmarks demonstrate the superior performance of NICE compared to the state-of-the-art methods in terms of explanation quality and image compression rate.

1 Introduction

Deep neural networks (DNNs) have become the de-facto performing technique in the field of computer vision [1], natural language processing [2], and speech recognition [3]. They require only limited domain knowledge to reach state-of-the-art performance given sufficient data and computation. However, the current DNNs are basically black-boxes with hundreds of layers of convolution, non-linearities, and gates, optimized solely for competitive performance, and our understanding of the reasoning of DNNs is lagged behind. DNNs' predictions may be backed up with a claimed high accuracy on benchmarks. However, it is human's nature not to trust them unless human experts are able to verify, interpret, and understand the reasoning of the system. Therefore, the usage of DNNs in real world decision-critical applications, such as surveillance cameras, drones, autonomous driving, medicine and legal, still must overcome a trust barrier. To address this problem, researchers have developed many different approaches to explain the reasonings of DNNs [4, 5, 6, 7, 8, 9, 10, 11, 12, 13, 14, 15]. Intuitively, interpretable explanations should be concise and coherent such that they will be easier for human to comprehend. However, most existing approaches do not take these requirements into account as manifested by the opaqueness and redundancies in their explanations [4, 6, 9, 10].

On the other hand, over 70% of internet traffic today is the streaming of digital media, and this percentage keeps increasing over the years [16]. It has been challenging for standard compression

algorithms, such as JPEG and PNG, to adapt to the growing demand. Recently, there is an increasing interest of using machine learning (ML) based approaches to improve the compression of images and videos [17, 18, 19, 20]. Rather than using manually engineered basis functions for compression, these ML-based techniques learn semantic structures and basis functions directly from training images and achieve impressive performance compared to the standard compression algorithms.

Usually, neural explanation and semantic image compression are addressed independently by two different groups of researchers. In light of the similarity between sparse explanation to image classification and sparse representation for image compression, in this paper we propose a deep learning based framework that integrates neural explanation and semantic image compression into an end-to-end training pipeline. With this framework, we can train a sparse mask generator to generate a concise and coherent mask to explain the prediction of CNN; subsequently, this sparse mask can be used to generate a mixed-resolution image with a very high compression rate, superior to the standard compression algorithms. This Neural Image Compression and Explanation (NICE) framework is critical to many real world decision-critical systems, such as surveillance cameras, drones and self-driving cars, that heavily rely on the deep learning techniques today. For these applications, the outputs of NICE: prediction, sparse mask / explanation, and the compressed mixed-resolution image can be stored or transmitted efficiently for decision making, decision interpretation and system diagnosis.

The main contributions of the paper are:

- We propose a deep learning based framework that unifies neural explanation and semantic image compression into an end-to-end trainable pipeline, which produces prediction, sparse explanation and compressed image in real time;
- The proposed L_0 -regularized sparse mask generator is trained in a weakly supervised manner without resorting to expensive dense pixel-wise annotations, and outperforms many existing explanation algorithms that heavily rely on backpropagation;
- The proposed mixed-resolution image compression achieves a very high compression rate compared to the standard compression algorithms, while retaining a similar classification accuracy.

2 The NICE Framework

Given a training set $D = \{(\mathbf{x}_i, y_i), i = 1, 2, \dots, N\}$, where \mathbf{x}_i denotes the i -th input image and y_i denotes the corresponding target, a neural network is a function $h(\mathbf{x}; \boldsymbol{\theta})$ parameterized by $\boldsymbol{\theta}$ that fits to the training data D with the goal of achieving good generalization to unseen test data. To optimize $\boldsymbol{\theta}$, typically the following empirical risk minimization (ERM) is adopted:

$$\mathcal{R}(\boldsymbol{\theta}) = \frac{1}{N} \sum_{i=1}^N \mathcal{L}(h(\mathbf{x}_i; \boldsymbol{\theta}), y_i), \quad (1)$$

where $\mathcal{L}(\cdot)$ denotes the loss over training data D , such as the cross-entropy loss for classification or the mean squared error (MSE) for regression. The goal of this paper is to develop an approach that can explain the prediction of a neural network $h(\mathbf{x}; \boldsymbol{\theta})$ in response to an input image \mathbf{x} ; meanwhile, to reduce storage or network transmission cost of the image, we'd like to compress the image \mathbf{x} based on the derived explanation above such that the compressed image $\tilde{\mathbf{x}}$ has the minimal file size while retaining a similar classification accuracy as the original image \mathbf{x} .

To solve these interdependent issues, we develop a Neural Image Compression and Explanation (NICE) framework that integrates explanation and compression into an end-to-end trainable pipeline as illustrated in Figure 1. In this framework, given an input image, a mask generator under the L_0 -norm and smoothness constraints generates a sparse mask that indicates salient regions of the image. The generated mask is then used to transform the original input image to a mixed-resolution image that has a high resolution in the salient regions and a low resolution in the background. To evaluate the quality of sparse mask generator and the compressed image, at the end of the pipeline a discriminator network (e.g., CNN) classifies the generated image for prediction. Finally, the prediction, sparse mask and compressed image can be stored or transmitted efficiently for decision making, interpretation and system diagnosis. The whole pipeline is fully differentiable and can be

trained end-to-end by backpropagation. In the sequel, we will introduce each of these components in more details.

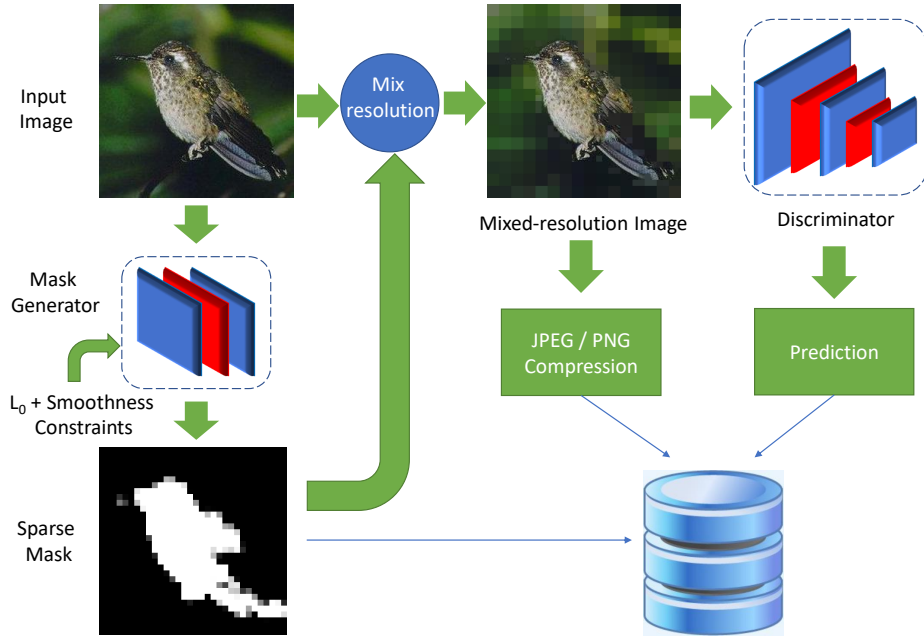


Figure 1: Overall architecture of NICE.

2.1 Sparse Neural Explanation

To correctly classify an image, a state-of-the-art CNN classifier does not need to analyze all the pixels in an image. Partially, this is because not all the pixels in an image are equally important for image recognition. For example, although the background pixels may provide some useful clues to recognize an object, it is the pixels on an object that play a decisive role for recognition. Based on this understanding, we'd like to learn a set of random variables (one for each pixel of an image) such that the variables on object pixels receive high values while the variables on background pixels receive low values. In other words, we want to learn a binary segmentation model that can partition pixels into object pixels and background pixels. To make our segmentation discriminative, we require the output of our model to be sparse/concise such that only the most important or influential pixels receive high values, and the remaining pixels receive low values. In addition, we expect the segmentation to be smooth/coherent within a small continuous region since most of natural objects usually have smooth appearances. We therefore request our neural explanation model to produce explanations that are concise and coherent. We will materialize these two requirements mathematically.

We model our neural explanation by attaching a binary random variable $z \in \{0, 1\}$ to each pixel of an image:

$$\tilde{x}_i = x_i \odot z_i, \quad z_i \in \{0, 1\}^P, \quad (2)$$

where z_i denotes a binary mask for image x_i , and \odot is an element-wise product. Furthermore, we define z_i^j the binary variable for pixel j of image x_i . We assume both image x_i and its mask z_i have the same spatial dimension of $m \times n$ or P pixels. After training, we wish z_i^j takes value 1 if pixel j is on object and 0 otherwise.

We regard \mathbf{z}_i as our explanation to the prediction of $h(\mathbf{x}_i; \boldsymbol{\theta})$ and learn \mathbf{z}_i by minimizing the following L_0 -norm regularized loss function:

$$\begin{aligned} \mathcal{R}(\boldsymbol{\theta}, \mathbf{z}) &= \frac{1}{N} \sum_{i=1}^N \left(\mathcal{L}(h(\mathbf{x}_i \odot \mathbf{z}_i; \boldsymbol{\theta}), y_i) + \lambda \|\mathbf{z}_i\|_0 \right) \\ &= \frac{1}{N} \sum_{i=1}^N \left(\mathcal{L}(h(\mathbf{x}_i \odot \mathbf{z}_i; \boldsymbol{\theta}), y_i) + \lambda \sum_{j=1}^P \mathbf{1}_{[z_i^j \neq 0]} \right), \end{aligned} \quad (3)$$

where $\mathbf{1}_{[c]}$ is an indicator function that is 1 if the condition c is satisfied, and 0 otherwise. Here, we insert Eq. 2 into Eq. 1 and add an L_0 -norm on the elements of \mathbf{z}_i , which measures *explicitly* number of non-zeros in \mathbf{z}_i or the sparsity of \mathbf{z}_i . By doing so, we'd like the masked image achieves the similar classification accuracy as the original image, while using as fewer pixels as possible. In other words, the sparse mask \mathbf{z}_i can produce a concise explanation to the prediction of the classifier (i.e., the first requirement). To optimize Eq. 3, however, we note that both the first term and the second term of Eq. 3 are not differentiable w.r.t. \mathbf{z} . Therefore, further approximations need to be considered.

Fortunately, we can approximate this optimization problem via an inequality from stochastic variational optimization [21]. That is, given any function $\mathcal{F}(\mathbf{z})$ and any distribution $q(\mathbf{z})$, the following inequality holds

$$\min_{\mathbf{z}} \mathcal{F}(\mathbf{z}) \leq \mathbb{E}_{\mathbf{z} \sim q(\mathbf{z})} [\mathcal{F}(\mathbf{z})], \quad (4)$$

i.e., the minimum of a function is upper bounded by the expectation of the function. With this result, we can derive an upper bound of Eq. 3 as follows.

Since $z_i^j, \forall j \in \{1, \dots, P\}$ is a binary random variable, we assume z_i^j is subject to a Bernoulli distribution with parameter $\pi_i^j \in [0, 1]$, i.e. $z_i^j \sim \text{Ber}(z; \pi_i^j)$. Thus, we can upper bound $\min_{\mathbf{z}} \mathcal{R}(\boldsymbol{\theta}, \mathbf{z})$ by the expectation

$$\tilde{\mathcal{R}}(\boldsymbol{\theta}, \boldsymbol{\pi}) = \frac{1}{N} \sum_{i=1}^N \left(\mathbb{E}_{q(\mathbf{z}_i | \boldsymbol{\pi}_i)} \left[\mathcal{L}(h(\mathbf{x}_i \odot \mathbf{z}_i; \boldsymbol{\theta}), y_i) \right] + \lambda \sum_{j=1}^P \pi_i^j \right). \quad (5)$$

Now the second term of the Eq. 5 is differentiable w.r.t. the new model parameters $\boldsymbol{\pi}$. However, the first term is still problematic since the expectation over a large number of binary random variables $\mathbf{z}_i \in \{0, 1\}^P$ is intractable, so is its gradient.

2.1.1 The Hard Concrete Gradient Estimator

Existing gradient estimators for this kind of binary latent variable models include REINFORCE [22], Gumble-Softmax [23, 24], REBAR [25], RELAX [26] and the hard concrete estimator [27], among which the hard concrete estimator is the one that is easy to implement and demonstrates superior performance in our experiments. We therefore resort to this gradient estimator to optimize Eq. (5). Specifically, the hard concrete gradient estimator employs a reparameterization trick to approximate the original optimization problem of (5) by a close surrogate loss function

$$\begin{aligned} \hat{\mathcal{R}}(\boldsymbol{\theta}, \log \boldsymbol{\alpha}) &= \frac{1}{N} \sum_{i=1}^N \left(\mathbb{E}_{\mathbf{u}_i \sim \mathcal{U}(0,1)} \left[\mathcal{L}(h(\mathbf{x}_i \odot g(f(\log \boldsymbol{\alpha}_i, \mathbf{u}_i)); \boldsymbol{\theta}), y_i) \right] + \lambda \sum_{j=1}^P \sigma \left(\log \alpha_i^j - \beta \log \frac{-\gamma}{\zeta} \right) \right) \\ &= \mathcal{L}_D(\boldsymbol{\theta}, \log \boldsymbol{\alpha}) + \lambda \mathcal{L}_C(\log \boldsymbol{\alpha}), \end{aligned} \quad (6)$$

with

$$\begin{aligned} f(\log \boldsymbol{\alpha}_i, \mathbf{u}_i) &= \sigma \left((\log \mathbf{u}_i - \log(1 - \mathbf{u}_i) + \log \boldsymbol{\alpha}_i) / \beta \right) (\zeta - \gamma) + \gamma, \\ g(\cdot) &= \min(1, \max(0, \cdot)), \end{aligned} \quad (7)$$

where $\sigma(t) = 1/(1 + \exp(-t))$ is the sigmoid function, \mathcal{L}_D measures how well the classifier fits to training data D , \mathcal{L}_C measures the expected number of non-zeros in \mathbf{z} , and $\beta = 2/3$, $\gamma = -0.1$ and $\zeta = 1.1$ are the typical parameters of the hard concrete distribution. For more details on the hard concrete gradient estimator, we refer the readers to [27]. With this reparameterization, the surrogate loss function (6) is differentiable w.r.t. its parameters.

2.1.2 Smoothness Regularization

The L_0 -regularized objective function developed above enforces the sparsity/conciseness of an explanation. To improve the coherence of an explanation, we introduce an additional smoothness constraint on the mask:

$$\begin{aligned} \mathcal{L}_S(\log \alpha) &= \frac{1}{N} \sum_{i=1}^N \mathbb{E}_{q(z_i | \log \alpha_i)} \left[\sum_{m,n=1}^{w,h} \left(\left| z_i^{m,n} - z_i^{m-1,n} \right| + \left| z_i^{m,n} - z_i^{m,n-1} \right| \right. \right. \\ &\quad \left. \left. + \left| z_i^{m,n} - z_i^{m-1,n-1} \right| + \left| z_i^{m,n} - z_i^{m-1,n+1} \right| \right) \right] \quad (8) \\ &\approx \frac{1}{N} \sum_{i=1}^N \sum_{m,n=1}^{w,h} \left(\left| y_i^{m,n} - y_i^{m-1,n} \right| + \left| y_i^{m,n} - y_i^{m,n-1} \right| + \left| y_i^{m,n} - y_i^{m-1,n-1} \right| + \left| y_i^{m,n} - y_i^{m-1,n+1} \right| \right), \end{aligned}$$

where $y_i^{m,n}$ is the expectation of random variable $z_i^{m,n}$ under the hard concrete distribution $q(z_i | \log \alpha_i)$, which can be calculated as:

$$y = \mathbb{E}_{q(z | \log \alpha)}[z] = \sigma \left(\log \alpha - \beta \log \frac{-\gamma}{\zeta} \right). \quad (9)$$

Note that this smoothness constraint penalizes the discrepancy of z among its four neighborhoods, and thus a coherence explanation is preferred (i.e., the second requirement). To avoid notational clutter, in Eq. 8 some of the boundary conditions are not rigorously checked, but we hope they will be apparent given the boundary context. With this additional regularization, our final objective is then a composition of three terms

$$\mathcal{L}(\theta_d, \log \alpha) = \mathcal{L}_D + \lambda_1 \mathcal{L}_C + \lambda_2 \mathcal{L}_S, \quad (10)$$

where λ_1 and λ_2 are the regularization hyperparameters that balance the data loss \mathcal{L}_D , the capacity loss \mathcal{L}_C and the smoothness loss \mathcal{L}_S . It's worthy noting that from now on we denote the parameters of classifier (discriminator) θ_d to distinguish it from the parameters of generator θ_g that will be introduced next.

After training, we get $\log \alpha$ for each input image x . At testing time, we employ the following estimator to generate a sparse mask:

$$\hat{z} = \min(\mathbf{1}, \max(\mathbf{0}, \sigma((\log \alpha)/\beta)(\zeta - \gamma) + \gamma)), \quad (11)$$

which is the sample mean of z under the hard concrete distribution $q(z | \log \alpha)$.

2.2 Semantic Image Compression

Upon receiving the sparse mask \hat{z} from above, we can use it to generate a mixed-resolution image for semantic image compression, as shown in Figure 1. Suppose that we have an input image x and a sparse mask $\hat{z} \in [0, 1]^P$, a mixed-resolution image can be generated by

$$\tilde{x} = M(x, \hat{z}) = x \odot \hat{z} + x_b \odot (1 - \hat{z}), \quad (12)$$

where x_b is a low resolution image that can be generated by subsampling from original image x with a block size of $b \times b$, which can be efficiently implemented by average pooling with a $b \times b$ filter and a stride of b . Here b is a tunable hyperparameter that trades off between the image compression rate and the classification accuracy of the classifier. In other words, the larger b is, the lower resolution images will be generated and thus a lower classification accuracy, and vice-versa. As we can see, when $b = 1$ the mixed-resolution image \tilde{x} is equal to the original image x ; when we use the image size as b , the mixed-resolution image \tilde{x} becomes a masked image with a constant value as background. When b is a value between these two extremes, we can generate mixed-resolution images of different levels of quality.

2.3 Sparse Mask Generator

The learning of sparse mask z discussed above is transductive, by which we can learn a mask for each image in training set D . However, this approach cannot generate masks for new images that are

not in the training set D . A more desirable approach is inductive, which can be implemented through a generator $G(x; \theta_g)$ such that it can produce a sparse mask given any image x as input. We model this generator as a neural network parameterized by θ_g .

To integrate this generator into an end-to-end training pipeline, we model this generator to output $\log \alpha$ given an input image x ; we can then sample a sparse mask z from the hard concrete distribution $q(z | \log \alpha)$, i.e., $x \xrightarrow{G(\cdot; \theta_g)} \log \alpha \xrightarrow{\text{sample}} z$. With this reparameterization, the overall loss function (10) becomes $\mathcal{L}(\theta_d, \theta_g)$, which can be minimized by optimizing the generator network θ_g and the discriminator network θ_d jointly with backpropagation. In the experiments, we employ a CNN as our sparse mask generator as CNNs are the de-facto technique today for image processing and understanding.

3 Related Works

Our work is primarily related to two active research areas of deep learning: neural explanation and semantic image compression. We therefore review them briefly in the next.

Neural Explanation In order to interpret DNN’s prediction and gain insights of their operations, a variety of neural explanation methods have been proposed in recent years [4, 5, 6, 7, 8, 9, 10, 11, 12, 28, 13, 14, 15, 29, 30]. These methods can be categorized based on whether it is designed to explain the entire model behavior (global interpretability) or a single prediction (local interpretability). The goal of global interpretability is to identify predictor variables that best explain the overall performance of a trained model. This class of methods are crucial to inform population level decision for rule extraction or knowledge discovery [14, 15]. Local interpretability aims to produce interpretable explanations for each individual prediction and the interpretability occurs locally. Local interpretability is by far the most explored area for generating explanations to DNNs [4, 8, 12, 29, 30]. The primary idea is to measure a change of the final prediction with respect to changes of input or getting feature attribution for the final prediction. Different local explanation methods implement this idea in different ways. For example, occlusion-based explanation methods remove or alter a fraction of input data and evaluate its impact to the final prediction [9, 10, 11, 5]. Gradient-based methods compute the gradient of an output with respect to an input sample by using backpropagation to locate salient features that are responsible to the prediction [6, 7, 28, 13]. Other local interpretability methods explain data instances by approximating the decision boundary of a DNN with an inherently interpretable model around the predictions. For example, LIME [8] and SHAP [12] sample perturbed instances around a single data sample and fit a linear model to perform local explanations. RTIS [9] extracts features from a DNN classifier and feeds extracted features and target label to an U-Net like generator to generate saliency maps for local explanations. L2X [29] learns a stochastic map based on mutual information that selects instance-wise informative features. Built on top of L2X, VIBI [30] selects instance-wise key features that are maximally compressed about an input and informative about a decision based on an information-bottleneck principle. NICE falls in the category of local interpretability and aims to produce concise and coherent local explanations similar to VIBI. But our method achieves brevity and comprehensiveness explicitly through an L_0 -norm regularization and an smoothness constraint, optimized via stochastic binary optimization.

Semantic Image Compression Standard image compression algorithms, such as JPEG [31] and PNG [32], have hard-coded procedures / components to compress images. For example, the JPEG compression first employs a discrete cosine transform (DCT) over each 8×8 image block, followed by quantization to represent the frequency coefficients as a sequence of binaries. The DCT can be seen as a generic feature extractor with a fixed set of basis functions that are irrespective of the distribution of the input images. Compared to standard image compression algorithms, the ML-based approaches [33, 34, 35, 36, 17, 19, 37, 20] can automatically discover semantic structures and learn basis functions from training images to achieve even higher compression rate. All of these ML-based approaches follow a similar structure of autoencoder, where an encoder is used to extract feature representation from images and a decoder is responsible to reconstruct images from the quantized representations. The main differences among these ML-based approaches are the architectures of encoder and decoder. While the majority of these algorithms [33, 36, 17, 19, 37, 20] employ CNNs as the encoder and decoder, some others explore recurrent networks such as LSTM and GRU [34, 35]. However, all of these methods are not sufficiently content-aware, except the work [18] from Prakash

et al. which is probably the most relevant to ours. While Prakash *et al.* adopt CAM [38] as the semantic region detector, we develop a principled L_0 -regularized sparse mask generator to detect the semantic regions and further compress images with mixed resolutions.

4 Experiments

To evaluate the performance of NICE, we conduct extensive experiments on two image classification benchmarks: MNIST [39] and Caltech256 [40]¹. MNIST is a gray-level image dataset containing 60,000 training images and 10,000 test images of the size of 28×28 for handwritten digits classification. Caltech256 is a high-resolution color image dataset containing 22,100 images from 256 classes of man-made and natural objects, such as plants, animals and buildings, etc. Since MNIST is a low-resolution image dataset, we use it mainly to demonstrate NICE’s performance on neural explanation. For the high-resolution images of Caltech256, we demonstrate NICE’s performance on neural explanation and image compression. All of our experiments are performed on NVIDIA Titan-Xp GPUs.

4.1 Implementation Details

Network architectures of the generators and discriminators used in the MNIST and Caltech256 experiments are provided in Table 1. Specifically, we employ LeNet5-Caffe² as the discriminator for the MNIST dataset, which achieves a 99% classification accuracy on the original MNIST dataset. We use ResNet-18 [1] as the discriminator for the Caltech256 dataset, which achieves a 78.3% classification accuracy. These two discriminators are the CNN classifiers we aim to explain.

Dataset	Generator	Discriminator
MNIST	Conv(1,1,3,1,1)	Conv(1,20,5,1,0) + ReLU + Maxpool(2) Conv(20,50,5,1,0) + ReLU + Maxpool(2) FC(800, 500) + ReLU FC(500, 10)
Caltech256	Conv(3,1,3,1,1) + ReLU + Maxpool(2) Conv(1,1,3,1,1) + ReLU + Maxpool(2) Conv(1,1,3,1,1) + Maxpool(2) Upsampling(8)	ResNet-18 FC(512, 256)

Table 1: Network architectures of the generators and discriminators used in the experiments.

Two approaches are used to train the NICE pipeline: (1) **Discriminator-fixed**: given a pre-trained discriminator (e.g., a CNN classifier), we freeze its parameters θ_d in the pipeline and only update the parameters of generator θ_g by optimizing the overall loss (10). In this case, the mask generator is trained to generate sparse explanation to the original discriminator. (2) **Discriminator-finetuned**: similar to discriminator-fixed except that the top few layers of the discriminator θ_d are finetuned. In this case, the discriminator can adjust its parameters to improve its predictions on the mixed-resolution images, and thus higher accuracy and compression rate are expected.

4.2 Explaining CNN’s Predictions

4.2.1 MNIST

We train the NICE pipeline on the MNIST dataset with **discriminator-fixed** in order to explain the predictions of the original discriminator. We initialize the discriminator of the NICE pipeline by a pre-trained LeNet5-Caffe on the original MNIST dataset. Different λ_1 s are used to generate sparse masks with different percentages of non-zeros (sparse explanations). λ_2 is set to 0 for all the MNIST experiments as the algorithm can generate coherent explanations without the smoothness constraint. The block size of the low resolution image x_b is set to 28, which means a constant background is used to generate the mixed-resolution images. We use the Adam optimizer [41] with a learning rate of 0.001 and a decay rate of 0.1 at every 5 epochs.

¹http://www.vision.caltech.edu/Image_Datasets/Caltech256/

²<https://github.com/BVLC/caffe/tree/master/examples/mnist>

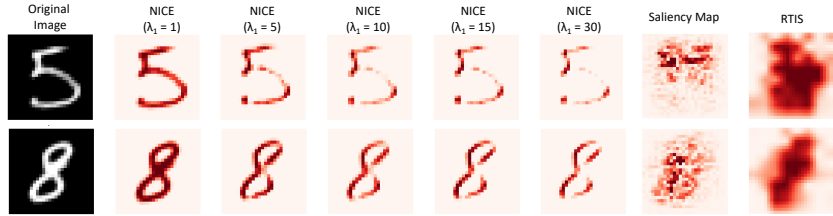


Figure 2: The sparse masks generated by NICE, Saliency Map [4] and RTIS [9] on the MNIST dataset. The dark red color represents high values (close to 1), indicating strong influence to the final decisions. By adjusting λ_1 of NICE, we can control the sparsity of the explanations.

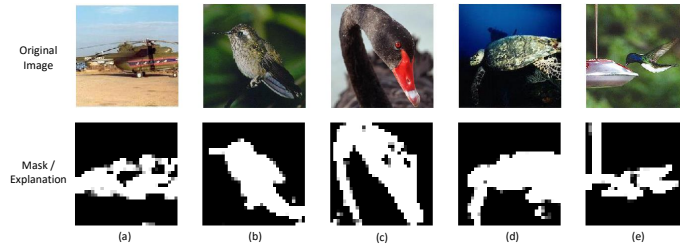


Figure 3: The sparse masks generated by NICE on the Caltech256 images. The predictions on (a,b,c,d) are correct and the prediction on (e) is incorrect. Even though the prediction is incorrect, the sparse mask of (e) provides an intuitive explanation why the discriminator predicts an image of “humming bird” as “bread maker”.

Figure 2 illustrates some example sparse explanations generated by NICE with different λ_1 s (and $\lambda_2 = 0$). As we can see, when λ_1 increases, the amount of non-zeros in the mask z decreases and NICE can produce sparser explanations to the final predictions. When $\lambda_1 = 1$, the explanations are almost identical to the input images, and when $\lambda_1 = 30$, the masks identify more influential regions for the final predictions. As a comparison, we also include the explanation results produced by Saliency Map [4] and RTIS [9]. While NICE highlights coherent regions over digits as explanations, Saliency Map, a backpropagation-based approach, identifies discontinued regions as explanations, which are quite blurry and difficult to understand. RTIS can yield coherent regions as explanations but it seems the regions identified are overly smooth. Apparently, the explanations produced by NICE are more concise, coherent and match well with how humans explain their own predictions.

4.2.2 Caltech256

Similarly, we train the NICE pipeline on the Caltech256 dataset with **discriminator-fixed** in order to explain the predictions of the original discriminator. We split the dataset into a training set of 16,980 images and a test set of 5,120 images. The images are then resized to 256×256 as inputs. We initialize the discriminator by a pre-trained ResNet-18 on the original Caltech256 dataset. We set $b = 256$ to generate the lowest resolution images x_b , and set $\lambda_1 = 5$ and $\lambda_2 = 0.01$ and train the pipeline by using the SGD optimizer with a learning rate of 0.001 and a cosine decay function.

Figure 3 demonstrates the sparse masks produced by NICE for different images of Caltech256. As we can see, the generated explanations are very concise and coherent, i.e., the sparse masks are mainly concentrated on the object regions, which align very well with our reasoning on these images. Additionally, the generated sparse masks also provide intuitive explanations when the discriminator makes mistakes. For example, as shown in Figure 3(e), the discriminator incorrectly predicts an image of “humming bird” as “bread maker”. The corresponding sparse explanation highlights the influential regions contributing the most to the discriminator’s prediction. Clearly, the discriminator utilizes both the regions of the hummingbird and the bird-feeder for the prediction, and the combination of the two regions confuses the discriminator and leads to the incorrect classification. This kind of explanations is very useful for system diagnosis: it provides greater visibility over unknown vulnerabilities and flaws, and can help to improve the performance of the system.

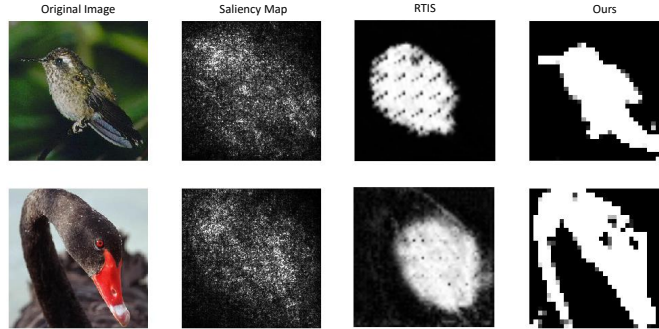


Figure 4: The sparse masks generated by NICE, Saliency Map [4] and RTIS [9] on the Caltech256 dataset. NICE highlights the whole body of object as the explanation instead of edges or scattered pixels as identified by Saliency Map, or overly-smooth regions as identified by RTIS.

Figure 4 illustrates the comparison of NICE with the two other explanation algorithms: Saliency Map [4] and RTIS [9] on the Caltech images. As we can see, our algorithm highlights the whole body of object as the explanation while Saliency Map typically identify edges or scattered pixels as the explanation. RTIS can identify coherent saliency regions of an image, however, those regions are overly smooth and cover large background regions³. Apparently, our explanations are more concise and coherent than those of the competing methods, and can preserve semantic contents of the images with a high accuracy. The superior performance of NICE on identifying semantic regions of images plays a critical role for image compression as we demonstrate next.

It’s also worth noting that due to the inductive training of the sparse mask generator NICE can produce explanations in nearly real time as it only requires forward evaluation of the generator network. For Saliency Map [4], it require both forward and backward propagations through the original discriminator to generate explanations, and thus are much more expensive than NICE.

4.3 Semantic Image compression

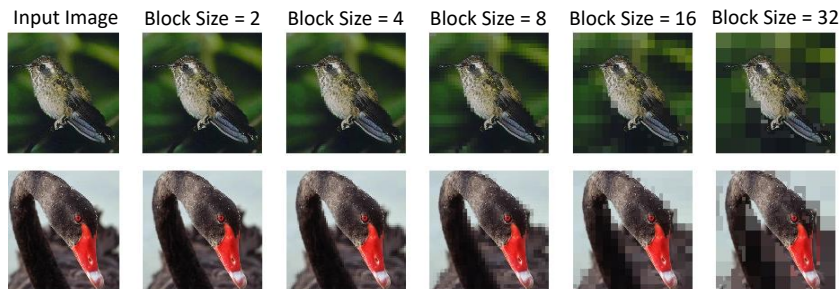


Figure 5: The mixed-resolution images generated by NICE with different block size b s. The salient regions of images are kept with the original high resolution, and the background regions are subsampled to reduce resolution. As the salient regions are identified accurately by NICE, the discriminator can still yield correct classification despite the background regions are compressed significantly.

Next, we evaluate the image compression performance of NICE on the Caltech256 images. As a start, we use the sparse masks identified by NICE in Figure 4 to generate a few mixed-resolution images via Eq. 12. Figure 5 illustrates some example mixed-resolution images generated with different block size b s. The mixed-resolution images maintain original high resolution in the salient regions identified by the sparse masks, and low-resolution in the background regions through subsampling. Thanks to the high accuracy of NICE on identifying salient regions, even when the background regions are

³See more example results on the ImageNet and CIFAR-10 images from the RTIS paper [9].

subsampled with a block size of 32, the discriminator can still successfully classify these images. As a result, high compression rate and high classification accuracy can be achieved simultaneously.

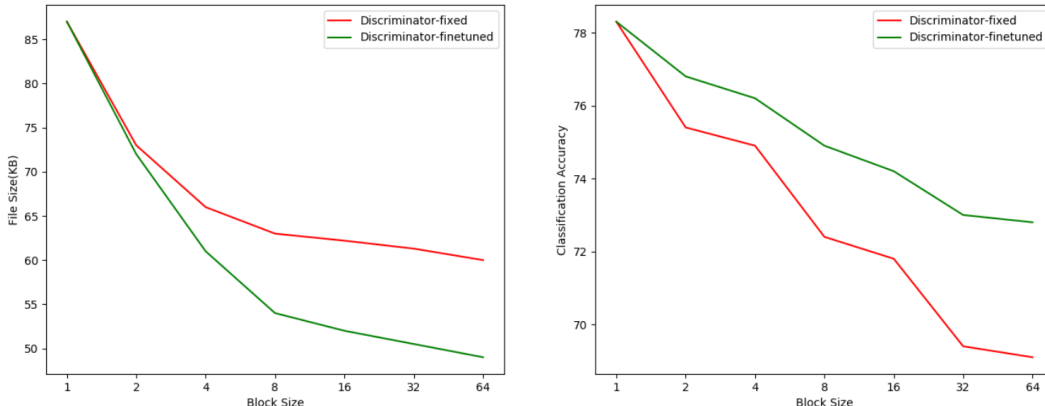


Figure 6: The evolution of (a) average file size of the PNG compressed image and (b) classification accuracy as a function of block size b . With the block size of 8, NICE achieves a 1.6x compression rate with a small 3.35% accuracy drop.

To quantitatively evaluate the trade-off between image compression rate and classification accuracy, we train both pipelines **discriminator-fixed** and **discriminator-finetuned**⁴ with $b = 16$ to generate sparse masks for each test image of Caltech256. After training, we generate mixed-resolution images with a different b in $\{1, 2, 4, 8, 16, 32, 64\}$. We then use PNG [32], a standard image compression algorithm, to store the generated mixed-resolution images and report the file sizes⁵. We also classify the mixed-resolution images with the discriminators to report classification accuracies. Figure 6 shows the average file size of compressed images and the corresponding classification accuracy as a function of block size b . As we can see, when the block size increases, the file size of the compressed images decreases (higher compression rate) and the classification accuracy also decreases (lower classification accuracy), and vis-versa. Comparing the results from both pipelines, the compression rate and classification accuracy of discriminator-finetuned are significantly better than those from discriminator-fixed. This is because discriminator-finetuned has an additional flexibility to finetune the discriminator and therefore higher compression rate and classification accuracy are expected. When the block-size is 8, discriminator-finetuned achieves a 1.6x compression rate (87KB vs. 54KB) with a small (3.35%) accuracy drop (78.30% vs. 74.95%), demonstrating the superior performance of NICE for neural explanation and image compression.

5 Conclusion

We propose a unified and end-to-end trainable framework NICE for neural explanation and semantic image compression. Compared to the competing explanation methods, such as Saliency Map and RTIS, the generated sparse masks from NICE are much more concise and coherent and align well with the reasoning of humans. In addition, due to its inductive training NICE can generate sparse explanations in real time, making it deployable to the real-time embedded systems. We conduct a series of experiments on multiple image classification benchmarks and demonstrate its improved explanation quality and image compression rate.

As for future work, we plan to investigate different image subsampling algorithms to generate x_b . We also plan to extend the technique developed here to other domains, such as text and bioinformatic data analysis.

⁴For discriminator-finetuned, we set the parameters of Conv-4, Conv-5 and the fully-connected layers of ResNet-18 to be trainable and freeze all the other layers.

⁵The reason that we choose PNG [32] instead of JPEG [31] for compression is because PNG is a lossless image compression algorithm. Therefore, the file size reduction of the mixed-resolution images can be 100% attributed to NICE, and the possible artifacts introduced by JPEG, a lossy compression, can be avoided.

References

- [1] Kaiming He, Xiangyu Zhang, Shaoqing Ren, and Jian Sun. Deep residual learning for image recognition. In *IEEE Conference on Computer Vision and Pattern Recognition (CVPR)*, pages 770–778, 2016.
- [2] Jacob Devlin, Ming-Wei Chang, Kenton Lee, and Kristina Toutanova. Bert: Pre-training of deep bidirectional transformers for language understanding. *arXiv preprint arXiv:1810.04805*, 2018.
- [3] Eric Battenberg, Jitong Chen, Rewon Child, Adam Coates, Yashesh Gaur, Yi Li, Hairong Liu, Sanjeev Satheesh, David Seetapun, Anuroop Sriram, and Zhenyao Zhu. Exploring neural transducers for end-to-end speech recognition. *arXiv preprint arXiv:1707.07413*, 2017.
- [4] Karen Simonyan, Andrea Vedaldi, and Andrew Zisserman. Deep inside convolutional networks: Visualising image classification models and saliency maps. *arXiv preprint arXiv:1312.6034*, 2013.
- [5] Matthew D Zeiler and Rob Fergus. Visualizing and understanding convolutional networks. In *European conference on computer vision (ECCV)*, pages 818–833, 2014.
- [6] Sebastian Bach, Alexander Binder, Grégoire Montavon, Frederick Klauschen, Klaus-Robert Müller, and Wojciech Samek. On pixel-wise explanations for non-linear classifier decisions by layer-wise relevance propagation. *PLoS one*, 10(7), 2015.
- [7] Chuang Gan, Naiyan Wang, Yi Yang, Dit-Yan Yeung, and Alex G Hauptmann. Devnet: A deep event network for multimedia event detection and evidence recounting. In *IEEE Conference on Computer Vision and Pattern Recognition (CVPR)*, pages 2568–2577, 2015.
- [8] Marco Tulio Ribeiro, Sameer Singh, and Carlos Guestrin. Why should i trust you?: Explaining the predictions of any classifier. In *Proceedings of the 22nd ACM SIGKDD international conference on knowledge discovery and data mining*, pages 1135–1144, 2016.
- [9] Piotr Dabkowski and Yarin Gal. Real time image saliency for black box classifiers. In *Advances in Neural Information Processing Systems (NIPS)*, pages 6967–6976, 2017.
- [10] Ruth C Fong and Andrea Vedaldi. Interpretable explanations of black boxes by meaningful perturbation. In *IEEE International Conference on Computer Vision (CVPR)*, pages 3429–3437, 2017.
- [11] Jiwei Li, Will Monroe, and Dan Jurafsky. Understanding neural networks through representation erasure. *arXiv preprint arXiv:1612.08220*, 2016.
- [12] Scott M Lundberg and Su-In Lee. A unified approach to interpreting model predictions. In *Advances in Neural Information Processing Systems (NIPS)*, pages 4765–4774, 2017.
- [13] Avanti Shrikumar, Peyton Greenside, and Anshul Kundaje. Learning important features through propagating activation differences. In *International Conference on Machine Learning (ICML)*, pages 3145–3153, 2017.
- [14] Chengliang Yang, Anand Rangarajan, and Sanjay Ranka. Global model interpretation via recursive partitioning. In *IEEE International Conference on Data Science and Systems (DSS)*, 2018.
- [15] Jonathan Ish-Horowicz, Dana Udwin, Seth Flaxman, Sarah Filippi, and Lorin Crawford. Interpreting deep neural networks through variable importance. *arXiv preprint arXiv:1901.09839*, 2019.
- [16] White paper: Cisco visual networking index: Forecast and trends, 2017–2022. Technical report, 2019.
- [17] Johannes Ballé, Valero Laparra, and Eero P. Simoncelli. End-to-end optimized image compression. In *International Conference on Learning Representations (ICLR)*, 2017.
- [18] Aaditya Prakash, Nick Moran, Solomon Garber, Antonella Dilillo, and James Storer. Semantic perceptual image compression using deep convolution networks. *2017 Data Compression Conference (DCC)*, Apr 2017.
- [19] Nick Johnston, Damien Vincent, David Minnen, Michele Covell, Saurabh Singh, Troy Chinen, Sung Jin Hwang, Joel Shor, and George Toderici. Improved lossy image compression with priming and spatially adaptive bit rates for recurrent networks. In *IEEE Conference on Computer Vision and Pattern Recognition (CVPR)*, pages 4385–4393, 2018.

- [20] Ken Nakanishi, Shin ichi Maeda, Takeru Miyato, and Daisuke Okanohara. Neural multi-scale image compression. In *Asian Conference on Computer Vision (ACCV)*, 2018.
- [21] Thomas Bird, Julius Kunze, and David Barber. Stochastic variational optimization. *arXiv preprint arXiv:1809.04855*, 2018.
- [22] Ronald J. Williams. Simple statistical gradient-following algorithms for connectionist reinforcement learning. *Machine Learning*, 8(3-4):229–256, May 1992.
- [23] Eric Jang, Shixiang Gu, and Ben Poole. Categorical reparameterization with gumbel-softmax. In *International Conference on Learning Representations (ICLR)*, 2017.
- [24] Chris J. Maddison, Andriy Mnih, and Yee Whye Teh. The concrete distribution: A continuous relaxation of discrete random variables. In *International Conference on Learning Representations (ICLR)*, 2017.
- [25] George Tucker, Andriy Mnih, Chris J. Maddison, John Lawson, and Jascha Sohl-Dickstein. Rebar: Low-variance, unbiased gradient estimates for discrete latent variable models. In *Advances in Neural Information Processing Systems (NIPS)*, 2017.
- [26] Will Grathwohl, Dami Choi, Yuhuai Wu, Geoff Roeder, and David Duvenaud. Backpropagation through the void: Optimizing control variates for black-box gradient estimation. In *International Conference on Learning Representations (ICLR)*, 2018.
- [27] Christos Louizos, Max Welling, and Diederik P. Kingma. Learning sparse neural networks through l_0 regularization. In *International Conference on Learning Representations (ICLR)*, 2018.
- [28] Ramprasaath R Selvaraju, Michael Cogswell, Abhishek Das, Ramakrishna Vedantam, Devi Parikh, and Dhruv Batra. Grad-cam: Visual explanations from deep networks via gradient-based localization. In *IEEE International Conference on Computer Vision (CVPR)*, pages 618–626, 2017.
- [29] Jianbo Chen, Le Song, Martin J Wainwright, and Michael I Jordan. Learning to explain: An information-theoretic perspective on model interpretation. *arXiv preprint arXiv:1802.07814*, 2018.
- [30] Seojin Bang, Pengtao Xie, Wei Wu, and Eric Xing. Explaining a black-box using deep variational information bottleneck approach. *arXiv preprint arXiv:1902.06918*, 2019.
- [31] Gregory K Wallace. The jpeg still picture compression standard. *IEEE transactions on consumer electronics*, 38(1), 1992.
- [32] Khalid Sayood. *Lossless compression handbook*. Elsevier, 2002.
- [33] Johannes Ballé, Valero Laparra, and Eero P Simoncelli. End-to-end optimized image compression. *arXiv preprint arXiv:1611.01704*, 2016.
- [34] George Toderici, Sean M. O’Malley, Sung Jin Hwang, Damien Vincent, David Minnen, Shumeet Baluja, Michele Covell, and Rahul Sukthankar. Variable rate image compression with recurrent neural networks. In *International Conference on Learning Representations (ICLR)*, 2016.
- [35] George Toderici, Damien Vincent, Nick Johnston, Sung Jin Hwang, David Minnen, Joel Shor, and Michele Covell. Full resolution image compression with recurrent neural networks. In *IEEE Conference on Computer Vision and Pattern Recognition (CVPR)*, pages 5306–5314, 2017.
- [36] Lucas Theis, Wenzhe Shi, Andrew Cunningham, and Ferenc Huszár. Lossy image compression with compressive autoencoders. *arXiv preprint arXiv:1703.00395*, 2017.
- [37] Mu Li, Wangmeng Zuo, Shuhang Gu, Debin Zhao, and David Zhang. Learning convolutional networks for content-weighted image compression. In *IEEE Conference on Computer Vision and Pattern Recognition (CVPR)*, pages 3214–3223, 2018.
- [38] Bolei Zhou, Aditya Khosla, Agata Lapedriza, Aude Oliva, and Antonio Torralba. Learning deep features for discriminative localization. In *IEEE Conference on Computer Vision and Pattern Recognition (CVPR)*, 2016.
- [39] Yann LeCun, Léon Bottou, Yoshua Bengio, Patrick Haffner, et al. Gradient-based learning applied to document recognition. *Proceedings of the IEEE*, 86(11):2278–2324, 1998.
- [40] Gregory Griffin, Alex Holub, and Pietro Perona. Caltech-256 object category dataset. 2007.

- [41] Diederik P Kingma and Jimmy Ba. Adam: A method for stochastic optimization. In *International Conference on Learning Representations (ICLR)*, 2015.